Enhancement of laminar mixing by an anchor impeller with rotationally reciprocating motion

Komoda, Yoshiyuki

Date, Tomoya

(Citation)
AIP Advances,12(1):015013

(Issue Date)
2022-01-01

(Resource Type)
journal article

(Version)
Version of Record

AIP Advances

Enhancement of laminar mixing by an anchor impeller with rotationally reciprocating motion

Cite as: AIP Advances **12**, 015013 (2022); https://doi.org/10.1063/5.0075750
Submitted: 18 October 2021 • Accepted: 16 December 2021 • Published Online: 10 January 2022

Yoshiyuki Komoda and Tomoya Date

Enhancement of laminar mixing by an anchor impeller with rotationally reciprocating motion

Cite as: AIP Advances 12, 015013 (2022); doi: 10.1063/5.0075750
Submitted: 18 October 2021 • Accepted: 16 December 2021 •
Published Online: 10 January 2022

Yoshiyuki Komoda[a] and Tomoya Date

AFFILIATIONS

Department of Chemical Science and Engineering, Graduate School of Engineering, Kobe University, Kobe, Hyogo, Japan

[a]**Author to whom correspondence should be addressed:** komoda@kobe-u.ac.jp. **Tel./Fax:** +81-78-803-6189. **Present address:** Department of Chemical Science and Engineering, Graduate School of Engineering, Kobe University, 1 1-1, Rokkodai-cho, Nada, Kobe, Hyogo 657-8501, Japan.

ABSTRACT

Rotationally reciprocating mixing, in which a plate impeller slowly rotates back and forth for only half a rotation, shows excellent fluid mixing performance at $Re > 40$. On the other hand, since vertical flow disappears at $Re < 10$, two-dimensional fluid mixing proceeds in the horizontal cross section of a cylindrical vessel, producing segmented mixing regions with a pair of central poor mixing zones. In this study, we investigated the usefulness of an anchor-type impeller in the expectation of enhancing two-dimensional fluid mixing under a laminar regime by utilizing the fluid flow through the central clearances. First, we examined the effect of the clearance size on the spreading behavior of tracer particles by numerical simulation. Time series of Poincaré sections are used to classify the tracer particles depending on their spreading behavior, which is then quantified by newly defined mixing ability. It is then elucidated that even a narrow central clearance could avoid the segmentation of the mixing region, while a vast central clearance produces additional isolated mixing regions in the clearance due to stable vortex flows. The tracer particles could uniformly spread in the entire circular cross section by increasing the impeller width and adjusting the flow rate in the central and wall clearances without segmentation. Furthermore, the experimental observation of streaklines could also demonstrate that the uniformity of the fluid mixing performance is improved considerably.

NOMENCLATURE

A	amplitude of the angular orientation (rad)
b	width of the impeller blade (mm)
D	diameter of the cylindrical vessel (mm)
d	width of the impeller (mm)
d_s	diameter of the mixing shaft (mm)
Ma	local mixing ability
N_{ave}	rotational speed averaged for one cycle of reciprocation (rps)
r	radial position of the tracer particle (mm)
Re	Reynolds number
T	period of rotational reciprocation (s)
θ	angular position of the tracer particle (rad)
μ	viscosity of the test fluid (Pa s)
ρ	density of the test fluid (kg m^{-3})
φ	angular orientation of the impeller (rad)

I. INTRODUCTION

Agitators are used widely for various purposes, such as the homogenization of fluids, the dispersion of particles, liquids, or gases, and the enhancement of chemical reactions. In many cases, impellers having various shapes are rotated at a high and constant speed to generate a three-dimensional turbulent flow in a vessel. However, the fluid flow near the vessel wall weakens and stagnates with increasing vessel size. The rotational speed usually increases further to enhance the fluid flow, and then, the fluid around the impeller is subjected to excessively high shear. On the other hand, in the manufacturing process of shear-sensitive materials, such as food,[1,2] liquid detergents, cosmetics, and cell culture fluids,[3,4] the fluid of interest is required to be agitated gently. Under laminar flow conditions, the fluid flow near the bottom and wall became stagnant, inducing the formation of a poor mixing region. Even if high

rotational speed stimulates the fluid flow in the whole of the vessel, isolated mixing regions (IMRs), having no fluid exchange with surrounding active mixing regions, are frequently observed.[5–7] One of the solutions to establish an effective laminar mixing process is the adoption of large impellers,[8,9] which consist of a small upper and large lower part. The vertical asymmetry contributes to generating a global fluid flow in a vessel without forming poor mixing regions even under laminar flow conditions. The asymmetry of the arrangement of the mixing shaft was the other method for enhancing fluid mixing, such as the inclination or eccentricity of the mixing shaft.[10–13]

These studies suggest that asymmetrical geometry is a key to improving mixing performance under laminar flow conditions. Therefore, rotational asymmetry must be one of the solutions to intensify laminar mixing. In other words, asymmetric impeller shape or non-uniform rotational motion is expected to establish an effective laminar mixing system. For example, the periodic change in the rotational speed could have avoided generating IMRs.[14] In this case, they showed that the stepwise change in the rotational speed was more effective rather than the sinusoidal change. Similarly, for the forward–reverse rotation[15] and angular oscillation,[16] where the rotational speed periodically changes from negative to positive, a frequent change in the rotational direction is advantageous to obtain higher mixing performance. Therefore, from these results, the impeller speed requires to change considerably for utilizing rotational asymmetry. Mainly in two-dimensional flow systems, the periodic change in the boundary condition has been studied intensively because chaotic laminar mixing is an academically interesting issue to intensify fluid mixing. Cavity flows, Bênard convections, and Moffat eddies are typical examples of chaotic mixing systems, which are induced by the superposition of fluctuation on the steady boundary conditions.[17–19] Aref also stated that two-dimensional chaotic mixing occurs even at very low Reynolds numbers by alternatively rotating two cylinders placed in a circular region.[20] In addition, the Poincaré section has been utilized to demonstrate excellent mixing performance by chaotic mixing for a figure-eight motion of a cylinder[21] and counter-rotating eccentric cylinders.[22] At very low Reynolds numbers, the inertial force weakens, and the flow field generated around the obstacle in the fluid becomes symmetric, which suppresses fluid mixing. Therefore, the mechanism of the baker's transformation by the asymmetry motion of the obstacle is essential for these chaotic mixing systems.

Agitators usually rotate the impellers having various shapes unidirectionally at a constant speed. Therefore, the asymmetry in the rotational direction by the alternative rotation of the impeller is expected to establish a chaotic mixing system. Then, we have proposed a rotationally reciprocating mixing,[23–26] where an impeller is rotated back and forth only by a half rotation at the frequency below 1 Hz. The overview of the experimental apparatus of the rotationally reciprocating mixing is shown in Fig. 1. For a considerable change in the impeller speed under a slow rotational motion, we chose a large plate impeller having a width of 75% of vessel diameter. At the Reynolds number of 40 or higher, the stretching and folding of a fluid element are repeated three-dimensionally, which is typical behavior in chaotic mixing systems shown as the left image of Fig. 1, realizing superior mixing performance. At a lower Reynolds number, the fluid flow in a vertical direction is negligible in the region away from the vessel bottom or liquid surface, indicating that the

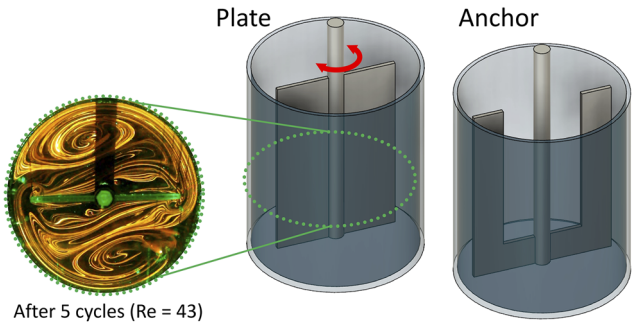

FIG. 1. Overview of a rotationally reciprocating mixing apparatus and the typical streakline for the plate impeller.

two-dimensional flow in the horizontal cross section governs fluid mixing. The acceleration of a large impeller is responsible for generating vortices in the horizontal cross section behind the impeller plate, and the size and position of the vortices change continuously due to the sinusoidal change in the rotational speed. As a result, it was found that a fluid element was still stretched and folded repeatedly, resulting in a typical fluid mixing for chaotic mixing in the horizontal cross section. However, at the much smaller Reynolds number of 10 or lower, the two-dimensional circular area consists of two active mixing regions and a pair of poorly mixed zones near the mixing shaft.

As far as using a large plate impeller, the semi-circular region in the horizontal circular cross section is bounded by non-slip boundaries of the impeller plate and vessel wall, and as a result, the central part remained poorly mixed. It was suspected that the removal of the non-slip boundary from the area near the poorly mixing area eliminates the poor mixing region, and the applicability of this mixing system can be expanded to a much smaller Reynolds number. Therefore, in the present study, a central clearance has been introduced to the plate impeller, that is, the switch from plate to anchor impeller, to enhance the fluid exchange beyond the impeller plate and to avoid the segmentation of the mixing region. First, the numerical investigation on the effects of the geometrical parameters of the anchor impeller on fluid mixing characteristics is conducted in terms of the Poincaré section. In terms of uniform spreading of a fluid element, the mixing ability is defined and utilized for the optimization of anchor impeller geometry for rotationally reciprocating mixing. Finally, experimental observation of streaklines in the horizontal cross section is carried out to confirm the validity of the optimized geometry of the anchor impeller.

II. NUMERICAL SIMULATION

Even at the Reynolds number of 10 or lower, fluid flow generated by a rotationally reciprocating impeller still contains vertical components near the vessel bottom or liquid surface. In an experimental observation, however, the tracer fluid injected at the middle height of the vessel mainly spread horizontally and slightly diffused in the vertical direction at the Reynolds number less than 40. This result means that radial and rotational flows dominate the fluid

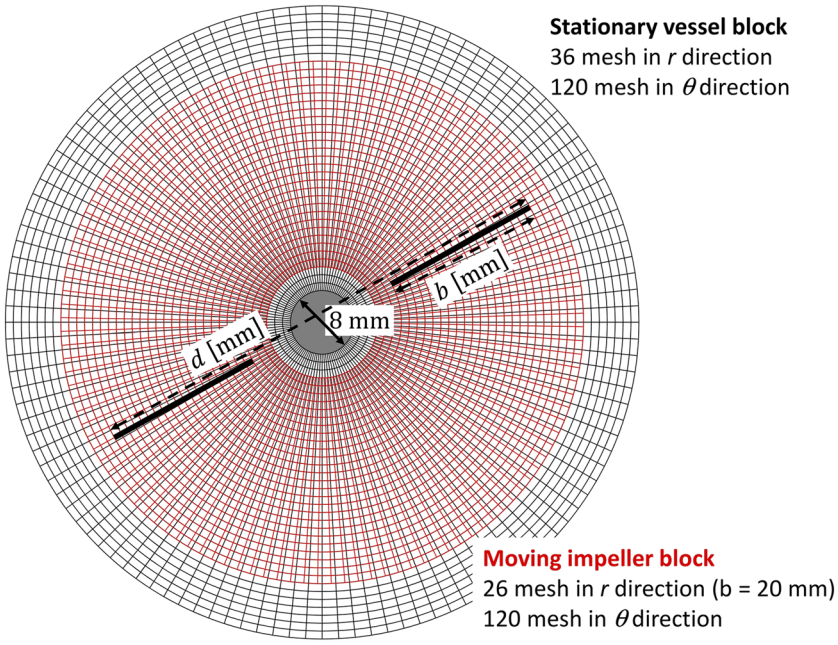

FIG. 2. Computational domain for rotationally reciprocating mixing.

mixing process, which is rarely affected by the vertical flow. Additionally, one of the purposes of this study is to confirm the effect of the anchor impeller on the segmentation of the mixing region and the formation of poor mixing zones in the horizontal plane. Therefore, the numerical simulation of the 2D laminar velocity field in the circular cross section induced by a rotationally reciprocating impeller has been conducted using computational fluid dynamics (CFD) software R-FLOW (R-flow corp., Japan).

Figure 2 shows the dimensions of the computational domain. The diameter of the cylindrical vessel is 80 mm, and that of the mixing shaft is 8 mm. The width of the plate impeller used in our previous studies is 60 mm. In the present study, the impeller width and blade width have been specified to represent the geometry of the anchor impeller. To investigate the effect of introducing a central clearance to the plate impeller, the blade width b was changed from 6 to 20 mm at the constant impeller width d of 60 mm. These anchor impellers are referred to as "small anchor impellers" hereafter. The effect of the impeller diameter on the mixing characteristics was also examined. Section IV C describes the details of the determination of the impeller diameter and center clearance for this study.

The computational domain is composed of the stationary vessel and moving impeller block. The regularly constructed mesh was generated for both blocks. The cell size is 1 mm in the radial direction and 3° in the azimuthal direction. Therefore, the stationary block is composed of 4320 cells. On the contrary, the moving block was an annular space, slightly larger than the area swept by the impeller plate by three meshes to inward and outward and rotated with the impeller. The logarithmically equal mesh was applied in the gap region, especially for narrow clearances at the center or at the wall.

A non-slip boundary condition has been applied to the surfaces of the impeller plate and mixing shaft. Equation (1) expresses the angular orientation of the impeller φ, where A and T represent the amplitude and reciprocation period, respectively. Those parameters are constant at $A = \pi/2$ and $T = 4$ s in this study. The rotational speed of the impeller and mixing shaft is the time derivative of Eq. (1) at each time step,

$$\varphi = A \cdot (1 - \cos(2\pi t/T)). \tag{1}$$

The inner surface of the vessel was also a non-slip boundary in the computation, and the thickness of the impeller plate was neglected for all computational conditions. A Navier–Stokes equation has been solved to compute the unsteady velocity field under a laminar flow condition using the SIMPLE algorithm. The SIMPLE algorithm generally suites well to calculate the steady complicated flow fields. In this study, the velocity field contains many vortices and changes slowly and periodically with time. Therefore, the SIMPLE algorithm was adopted to calculate the complicated velocity field precisely. The periodicity of the velocity field in each reciprocation cycle has been confirmed by superposing the variation of the radial and rotational velocity components at several points. As a result, the periodic velocity field with impeller motion has been confirmed for any condition after ten cycles of computation. Equation (2) defines the Reynolds number for the rotationally reciprocating plate impeller,

$$\mathrm{Re} = \rho N_{\mathrm{ave}} d^2/\mu \ (N_{\mathrm{ave}} = 2A/\pi T), \tag{2}$$

where d is the width of the impeller and that of the anchor impeller was a representative length regardless of the central clearance like the previous study.[27] The density of test fluids ρ was constant at 1.2×10^3 kg m^{-3}, while the viscosity μ was changed from 0.12 to 0.18 Pa s to adjust $Re = 9$ regardless of the impeller width. We obtained a series of velocity fields in one cycle of reciprocation after attaining a periodically stable state. It contains 200 sets of

velocity fields because of the calculation time step of 0.02 s and the reciprocating period of 4 s.

The mixing characteristic was studied using tracer particles, which moved according to numerically obtained velocity fields. Although a tracer particle moves considerably within one cycle of reciprocation, it may return to its original position after the cycle. Therefore, the trajectory of tracer particles will not give information about the degree of mixing. Instead, the change of the particle position at the end of each cycle should be valuable for the mixing characteristic of a periodic fluid flow. Singh *et al.* proposed the discrete intensity of segregation as a measure of the deviation of the local concentration, which is based on the number density of tracer particles in each computational cell.[28] In contrast, we pay attention to the fraction of the area occupied by a single tracer particle until the end of the measuring time. The annular region bounded by the mixing shaft and vessel wall was newly divided into 20 in the angular direction and 10 in the radial direction for this purpose, which is different from computational mesh. The circular cross section consists of 200 annular sectors, as shown in Fig. 3. Since the probability of the location of a tracer particle in a single annular sector depends on the size, the annular region has been divided equally so that each annular sector has the same area. Tracer particles were placed initially at the center of each sector. Then, we computed the positions of each tracer particle for 200 cycles and put the tracer particles at the end of each cycle in the same annular region. It is known as a Poincaré section, which, for example, emerges the area not occupied by the tracer particle.

We defined a mixing ability, Ma, to evaluate the mixing performance quantitatively based on the time variation of Poincaré sections. Equation (3) expresses the fraction of sectors occupied by a tracer particle at the end of each cycle until the end of the calculation period, which is a local mixing ability, M_a^k. The kth tracer particle located initially at the sector of (i_0^k, j_0^k) moved to the sector of (i_n^k, j_n^k) at the end of the nth cycle, as shown in Fig. 3. $\delta_{i,j}^k(n) = 1$ means that the tracer particle takes the position in the sector of (i,j) until the end of the nth cycle. On the contrary, $\delta_k^{i,j}(n) = 0$ indicates that the tracer particle is always located outside of the sector of (i,j). Since the computational domain consists of 200 sectors in this study, the local mixing ability is the minimum of 0.005 (=1/200) when the tracer particle moves only within an initial sector. $M_a^k(n) = 1$ means that the tracer particle has been placed in all by the end of 200 cycles. Note that it takes at least 200 periods for a tracer particle to attain $M_a^k(n) = 1$. Therefore, increasing the local mixing ability means spreading the tracer particles in the annular region at the fixed impeller position. In other words, if there is a region where the tracer particles cannot enter, the local mixing ability of those particles will be less than one. However, this does not directly mean that the mixing performance of the sector is low, but that the particles initially placed in the sector spread only partially. Additionally, Eq. (4) defined the average mixing ability, $\langle M_a \rangle$,

$$M_a^k(n) = \sum_{i=1}^{i_{\max}} \sum_{j=1}^{j_{\max}} \delta_{i,j}^k(n) / i_{\max} j_{\max}, \tag{3}$$

$$\langle M_a \rangle(n) = \sum_{k=1}^{k_{\max}} M_a^k(n) / k_{\max}. \tag{4}$$

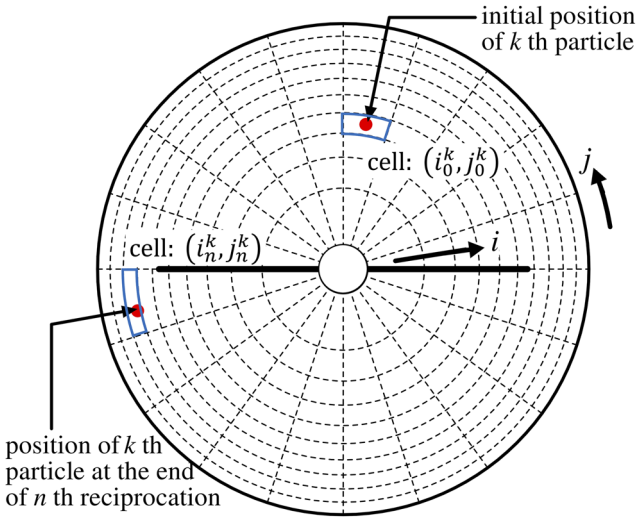

FIG. 3. Position of the tracer particle to calculate the mixing ability.

III. EXPERIMENTS

An impeller (height: 100 mm) is placed at the center of a flat-bottomed cylindrical vessel (D = 80 mm) with an off-bottom clearance of 2 mm. The impellers are attached to a stainless shaft having a diameter of 8 mm, connected to a stepper motor. The stepper motor is controlled by a high-performance motion control board so that the impeller slowly rotates back and forth. The angular orientation of the impeller is the same with numerical simulation and expressed by Eq. (1). Figure 4 shows the top and side views of impellers used in this study. We used an aqueous solution of glycerol as a test fluid. The glycerol concentration is from 67 to 72 wt. %, depending on the impeller width. The solution viscosity is identical to that is specified in the numerical simulation. The difference in densities of those solutions is negligible. We conducted all experiments at room temperature (~25 °C).

Figure 5 shows a schematic image of the experimental setup. An impeller and vessel made of transparent acrylic resin are used in the present study. The liquid level of the test fluid was 80 mm. The test fluid colored by Rhodamine B was injected continuously at the height of 70 mm from the vessel bottom using a stainless nozzle and syringe pump. The injection point is near the outer edge of the plate or the small anchor impeller. However, the injection point for the anchor impeller was the inner edge. The angular position of the injection point was $3\pi/4$. Although the shape of the boundary of active mixing regions deforms with impeller motion for the plate or the small anchor impeller, the injection point was always in one of the active mixing regions. It was confirmed in advance by experiment that the tracer fluid spread mainly in the horizontal plane at the injected height and diffused slightly in the vertical direction. Therefore, a semi-conductor green laser sheet irradiates the horizontal circular cross section, including the tracer injection point. The streakline was observed from the vessel bottom using a mirror and

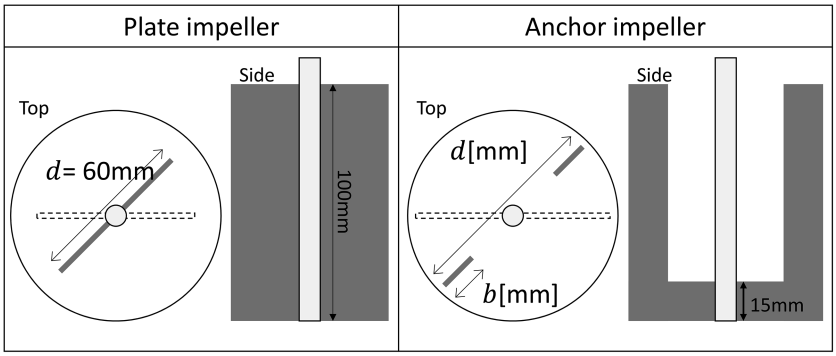

FIG. 4. Geometries of the plate and anchor impellers.

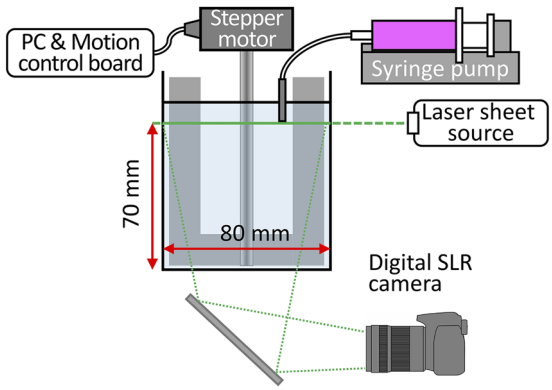

FIG. 5. Mechanics of the rotational reciprocation and optics for the streakline observation.

recorded as a movie using a digital single-lens reflex (SLR) camera (EOS Kiss X6i and 18–135 mm lens, Canon).

IV. RESULTS AND DISCUSSION

A. Mixing characteristics of plate impeller

Figure 6 lists Poincaré sections for a plate impeller after 100 cycles of reciprocation, which describe the mixing characteristics. Poincaré sections are usually used to distinguish between chaotic mixing zones and islands. However, in the present system, it is found that the chaotic zone was not uniform and separated into two crescent-shaped regions. Additionally, the separation of the chaotic zone can be suppressed by optimizing impeller geometry. Therefore, the tracer particles are colored differently depending on the behavior. The initial positions of the tracer particles for each Poincaré section are on semi-circular arcs in the upper semi-circle with different radii, represented by larger filled circles. Thus, one can find that tracer particles, initially located near the vessel wall, produced the crescent-shaped Poincaré section ($2r/D = 0.922$), where r represents the radial position of a tracer particle. With decreasing radius, the particle density of tracer particles in the upper crescent-shape region decreases, and the lower crescent-shape region emerges instead. At the same time, some tracer particles exhibit orbital motions near the mixing shaft. Precisely, most tracer particles move around in either the upper or lower crescent-shape region or on the orbit, though the exchange between two crescent-shaped regions or the release from the orbit rarely occurs. Therefore, the tracer particles were colored differently depending on their motion. Blue tracer particles are always in the upper crescent-shape region, red ones are in the lower region, and green ones circulate along the orbit near the mixing shaft. As a result, the color difference between blue and red clearly distinguishes the boundary of the upper and lower crescent-shaped regions. Additionally, the central vacant zone emerged, in which green tracer particles circulate.

However, some tracer particles show unpredictable behavior. For example, in the case of 2r/d = 0.393, a blue tracer particle is released from the orbital motion, travels along with the impeller plate, and finally enters the upper crescent-shaped region. Furthermore, as for the tracer particles at 2r/d = 0.922, the behavior of the green tracer particles was quite different from other green ones initially positioned inner. The green tracer particle originally placed on the edge of the crescent-shaped area translated along the boundary for several cycles and then involved into the orbit expressed by dark-green lines. Meanwhile, the other green tracer particle traveled along the wall, on the perimeter, and finally trapped into the opposite orbit, shown by light-green lines. In either case, the tracer particle travels along the boundary of the crescent-shaped region and then enters the circulating zone from the nearest point.

In conclusion, the Poincaré section reveals that a horizontal annular plane consists of four regions, i.e., two crescent-shaped active mixing regions and two central poor mixing zones facing each other across the impeller plate. A tracer particle in the crescent-shaped region can get into the central poor mixing zone and vice versa. However, since tracer particles exchange only by passing through a narrow path, fluid will not be mixed uniformly in the entire region.

Figure 7 lists the Poincaré sections at the end of different cycles using several tracer particles that initially have the same angular position but different radially to investigate the spreading behavior of tracer particles. The variable θ represents the angular position of a tracer particle. The green tracer particle generates the orbit even after 25 cycles, whereas other tracer particles spread randomly in either crescent-shaped region. To quantify the spreading behavior of each tracer particle, we computed local mixing abilities for each tracer particle, which are shown in the right of Fig. 7 as a function of cycles. In the case of the green tracer particle, the local mixing ability has reached 0.045 after 20 cycles and did not change any further.

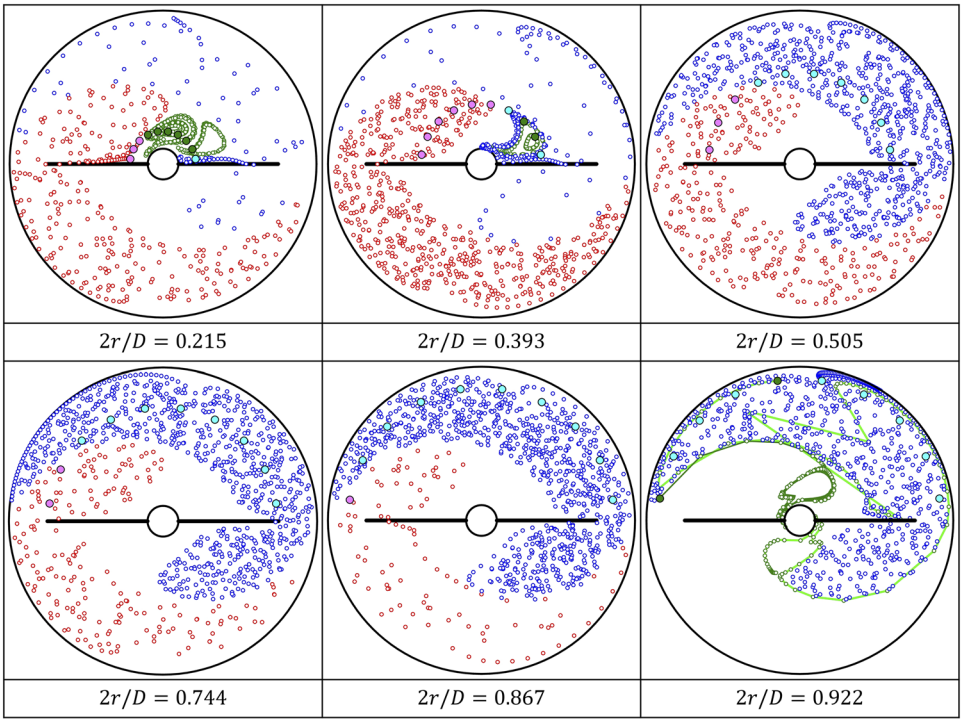

FIG. 6. Poincaré sections of the plate impeller after 100 cycles of reciprocation. The initial positions of tracer particles are indicated by large circles. The tracer particles are colored differently depending on the spreading behavior. Blue and red tracer particles spread in the crescent-shaped chaotic mixing regions, but green tracer articles form isolated mixing regions.

This behavior corresponds to the orbit of the green tracer particle occupied nine sectors out of 200. However, the local mixing abilities of other tracer particles in the crescent-shaped region were increased monotonically for the first 100 cycles and reached 0.35–0.45 after 200 cycles. Since the horizontal circular cross section comprises two major crescent-shape regions and minor central poor mixing zones, the area of the crescent-shaped region is slightly smaller than half of the computational domain.

Consequently, the local mixing ability of tracer particles spreading in the crescent-shape region attains ~0.4. Furthermore, the local mixing ability of the tracer particles in the crescent-shape region increased similarly regardless of the initial position though they deviated after 100 cycles. Therefore, the local mixing ability distribution indicates the uniformity of mixing performance, and the increasing trend of the average mixing ability means how fast the tracer particle spread in the area of interest.

B. Effect of blade width of small anchor impeller

We examined the effect of the central clearance of the small anchor impeller on the formation of the central poor mixing zone. Figure 8 shows Poincaré sections of tracer particles initially placed on two half arcs with different radii when using the small anchor impellers with varying blade widths. In these figures, the rules of filling and coloring tracer particles were the same as those in Fig. 6. With decreasing blade width, some tracer particles go across the vague boundary of the crescent-shaped region. Orange tracer particles indicate that they can take positions in upper and lower areas. In the case of the plate impeller, green particles near the shaft are in the central poor mixing zone, and blue and red particles indicate the segmentation of the active mixing region.

In contrast, introducing a 6 mm central clearance (b = 20 mm) eliminates the poor mixing zones while leaving the segmentation of active mixing regions. Nevertheless, some tracer particles colored in orange can spread in the whole area, suggesting the enhancement of mixing between those active mixing regions. However, this segmentation could not avoid up to the central clearance of 20 mm (b = 6 mm). More critical thing accompanied by the expansion of clearance is the formation of several pairs of regions unfilled by tracer particles at the blade width less than 13 mm. In these cases, green tracer particles showed orbital motion in active mixing regions, suggesting the formation of an isolated mixing region (IMR). Generally, steady rotational type impellers are well known to produce a pair of stable donut-shaped IMRs under laminar flow conditions. In contrast, the IMR for rotationally reciprocating anchor impeller changes its position and shape with impeller motion. The dynamics of these IMRs are a fascinating topic in future work.

For more quantitative discussion, Fig. 9 plots the time variation of the average mixing ability and the cumulative distribution of the local mixing ability at the end of 100 cycles. Small anchor impellers with narrow blades showed a slow increase in the average mixing

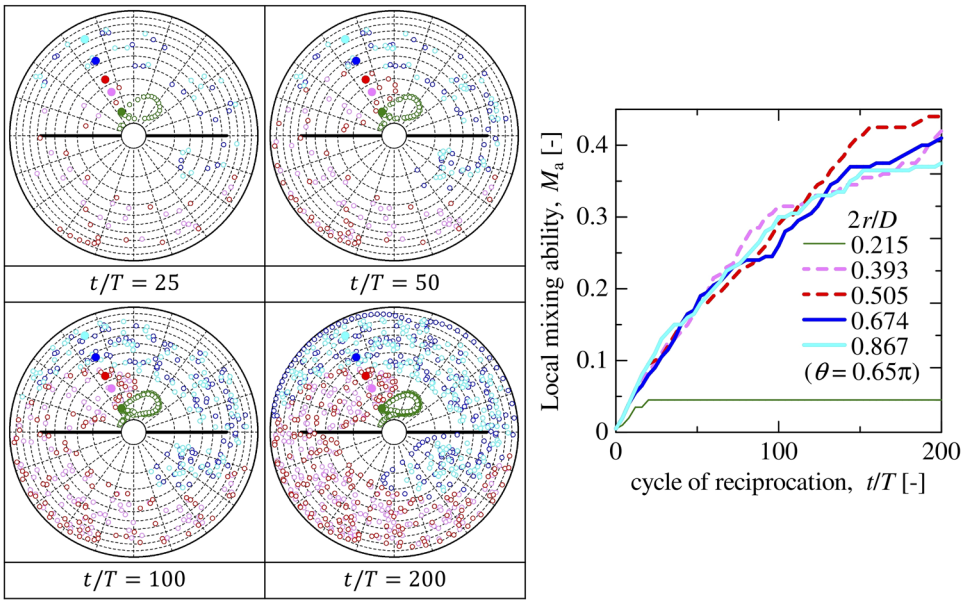

FIG. 7. Time series of Poincaré sections and local mixing ability for the plate impeller.

ability. A significant fraction of tracer particles taking a small local mixing ability (Ma < 0.1) in the cumulative distribution is the reason to show the poor mixing performance. On the contrary, the average mixing ability of small anchor impellers with a large blade is more remarkable than that of the plate impeller after 50 cycles. The average mixing ability approached 0.5 thanks to orange tracer particles, which spread in either active mixing region. However, even in the cumulative distribution, no significant differences could be observed

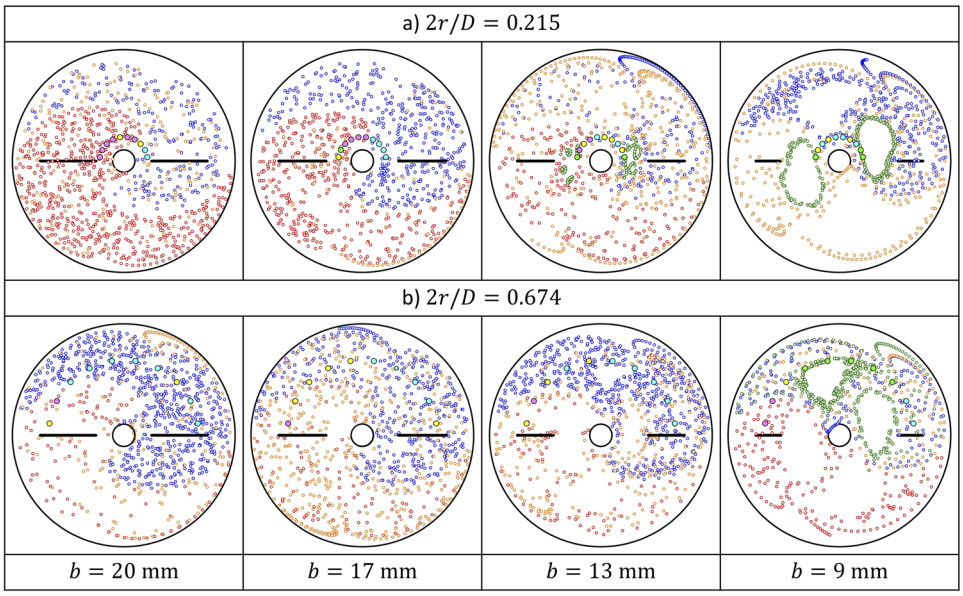

FIG. 8. Poincaré section of small anchor impellers after 100 cycles using tracer particles initially placed on arcs with different radii; filled circles indicate their initial positions; the color indicates the difference in the spreading behavior.

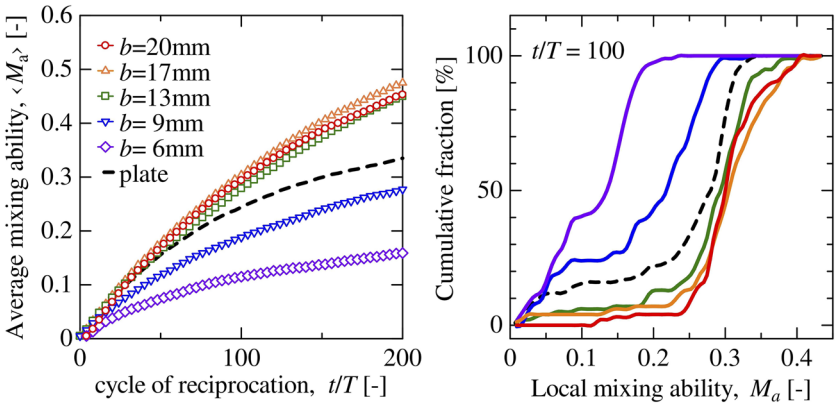

FIG. 9. Effect of the blade width of small anchor impellers on the increasing trend of the average mixing ability and the cumulative distribution of the local mixing ability.

among small anchor impellers with a blade width of more than 13 mm.

Figure 10 summarizes the maps of the local mixing ability for those impellers at the end of 100 cycles. It is reasonable that a tracer particle that always locates in a poor mixing zone shows a low local mixing ability. However, the local mixing ability becomes low if another tracer particle is initially placed outside but enters the poor mixing zone. At the blade width of 6 mm, the local mixing ability was low in the four central large zones and the two thin regions along the vessel wall. As the blade width increased to 17 mm, the central zones shrank and finally disappeared, while the thin regions were not changed significantly. However, any tracer particles in the entire region do not show low mixing ability for the blade width of 20 mm. Therefore, the central poor mixing zone formation is avoidable by introducing the central clearance. However, a narrow blade cannot sweep sufficient fluid and produce a sufficiently strong vortex, resulting in isolated mixing regions. Section IV D will describe the effect of the impeller geometry on the flow field generated in the horizontal plane.

C. Effect of impeller width of anchor impeller

The extension of the impeller width keeping the central clearance constant, indicating the enlargement of the blade width, must

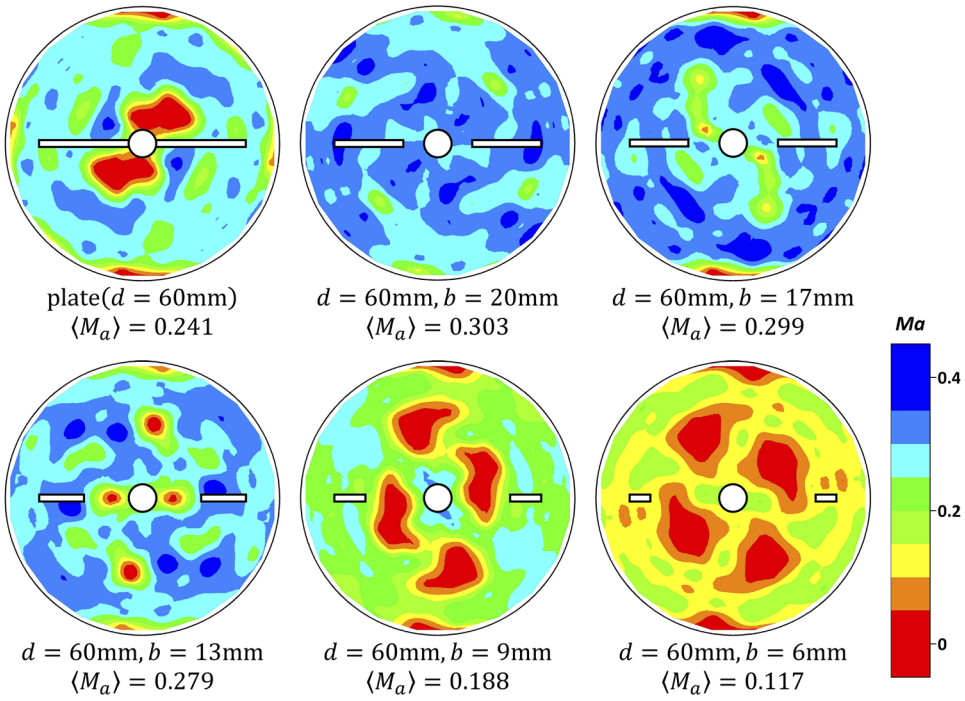

FIG. 10. Local mixing ability map for small anchor impellers after 100 cycles.

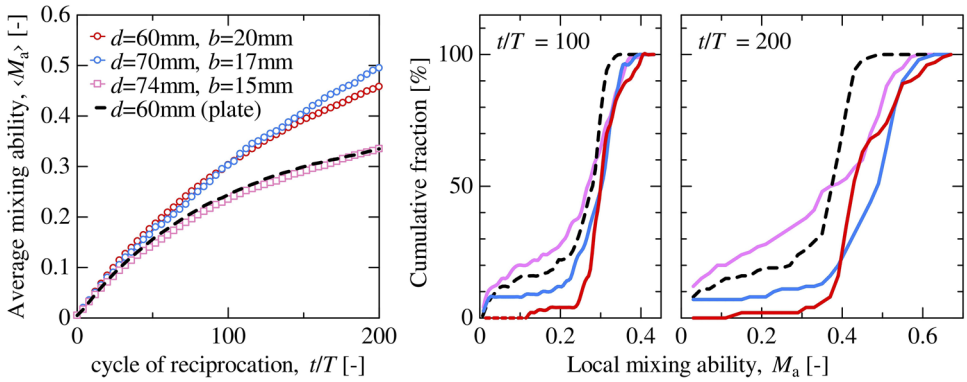

FIG. 11. Increasing trend of the average mixing ability and the cumulative distribution of the local mixing ability of optimized anchor impellers.

significantly increase the torque or power consumption. Therefore, the geometry of anchor impellers was determined to show power consumption roughly the same as the plate impeller. Assuming that the drag stress τ applied to the impeller blade is uniform over the impeller plate, the torque exerted on the mixing shaft per unit length is calculated by Eq. (5). Therefore, we decided the geometry of the anchor impeller as $d = 70$ mm$(b = 17$ mm$)$ or $d = 74$ mm$(b = 15$ mm$)$ so that they show the torque roughly the same as that of the plate impeller $(d = 60$ mm and $b = 26$ mm$)$. We have obtained the results that the swept area by the rotationally reciprocating plate impeller should be approximately half the circular area to conduct fluid mixing efficiently. The swept area ratios of these anchor impellers are roughly 55%, which are appropriate for efficient fluid mixing,

$$M = \int_{d/2-b}^{d/2} \tau dr \cdot r = \tau/2 \cdot b(d-b). \tag{5}$$

The change of the mean value and the cumulative distribution of the local mixing ability for those anchor impellers were compared with the small anchor and plate impellers, as shown in Fig. 11. When the impeller width was excessively increased to $d = 74$ mm, the average mixing ability was significantly reduced and coincided with the plate impeller. The widest anchor impeller produced a broad distribution in the local mixing ability, suggesting that the mixing performance is inhomogeneous over the area of interest. On the other hand, there was no significant difference in the average mixing ability between the $d = 70$ mm anchor impeller and the small anchor impeller. The distribution of the local mixing ability of the small anchor impeller showed that almost no tracer particle showed $Ma < 0.3$ and that roughly 20% of tracer particles did $Ma > 0.5$ after 200 cycles. In contrast, $Ma < 0.3$ for 10% of tracer particles and $Ma > 0.5$ for 40% of tracer particles in the case of the anchor impeller of $d = 70$ mm. Therefore, a more uniform mixing performance is obtainable when using the small anchor impeller with a narrow

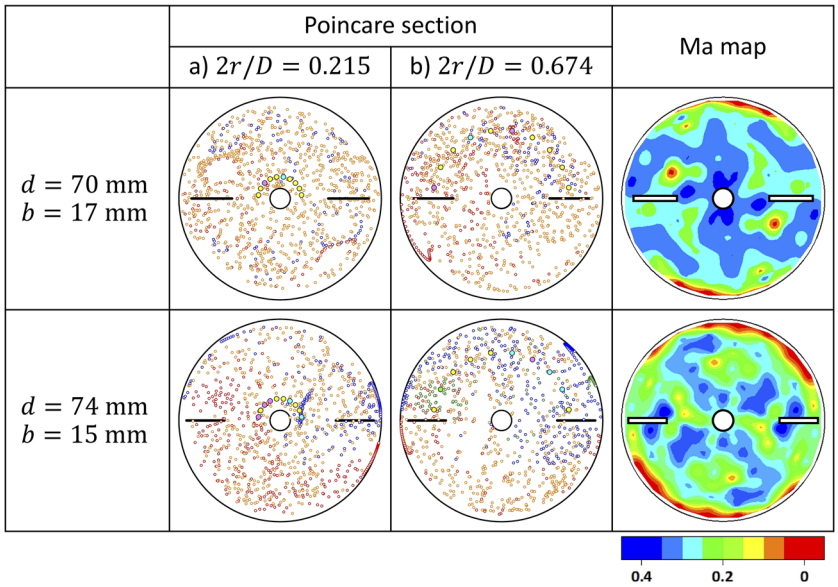

FIG. 12. Poincaré section of optimized anchor impellers after 50 cycles of reciprocation.

central clearance among the impellers investigated in this study in terms of mixing ability.

Remember that the small anchor impeller divides the circular cross section into two segments. Figure 12 compares the Poincaré sections for the anchor impellers after 100 cycles to elucidate the area of interest segmentation. The figure also includes the local mixing ability maps. In the case of d = 70 mm, many tracer particles colored by orange spread over the entire region, and no obvious segmentation occurs. However, there are vacant zones adjacent to the impeller plate, where no tracer particle takes the position. The zones show good agreement with the zero local mixing ability region in the map, and some of the orange tracer particles circulate similar to that observed for the small anchor impellers with narrow blades. Therefore, enlargement of the central clearance induces generating isolated mixing regions. In the case of d = 74 mm, on the other hand, the mixing area is again weakly segmented but does not contain isolated mixing regions. However, the most significant difference from the d = 70 mm anchor impeller is the insufficient uniformity of tracer particles. Considering the gap between the impeller tip and vessel wall, this may be due to insufficient fluid exchange through the wall clearance.

D. Velocity field induced by rotationally reciprocating impellers

The effect of the impeller geometry on fluid flow was studied to elucidate an appropriate velocity field to avoid the poor mixing zones and the mixing region segmentation. Although the velocity field changes continuously with the impeller position during one cycle of reciprocation, a characteristic difference was found at the impeller angular position of $\varphi = \pi/3$ as shown in Fig. 13. In the case of the plate impeller, a rotational motion governs the velocity field. However, the fluid flow in front of the outer part of the impeller plate contains a weak radial component, and a pair of weak vortices emerged in the gap between the impeller tip and vessel wall. The asymmetry shall generate an asymmetry velocity field between the forward and reverse impeller motions, progressing fluid mixing. However, a weak asymmetry in the internal area is the reason to form the poorly mixing zone. In the case of small anchor impellers, although vortex flow in the wall gap seems not to be affected by the blade width, other vortices are produced in the central clearance. By expanding the clearance, the vortex becomes enormous, but its center will not be away from the inner edge of the blade. Consequently, a fluid element around the vortex rotated in one direction in the first half period and did in the opposite direction in the following half period and eventually formed isolated mixing regions. Therefore, a small central clearance produced weak asymmetry with no vortices around the mixing shaft, enhancing fluid mixing in the central zone. However, since the velocity field dominating overall fluid mixing is similar between the small anchor and plate impellers, the mixing region is still segmented.

On the other hand, with increasing impeller width, the vortex flow for the anchor impeller at the wall gap was suppressed significantly. As a result, fluid flow through the central clearance was strengthened, which enlarged central vortex flow and induced the retardation of the vortex center against the impeller inner edge.

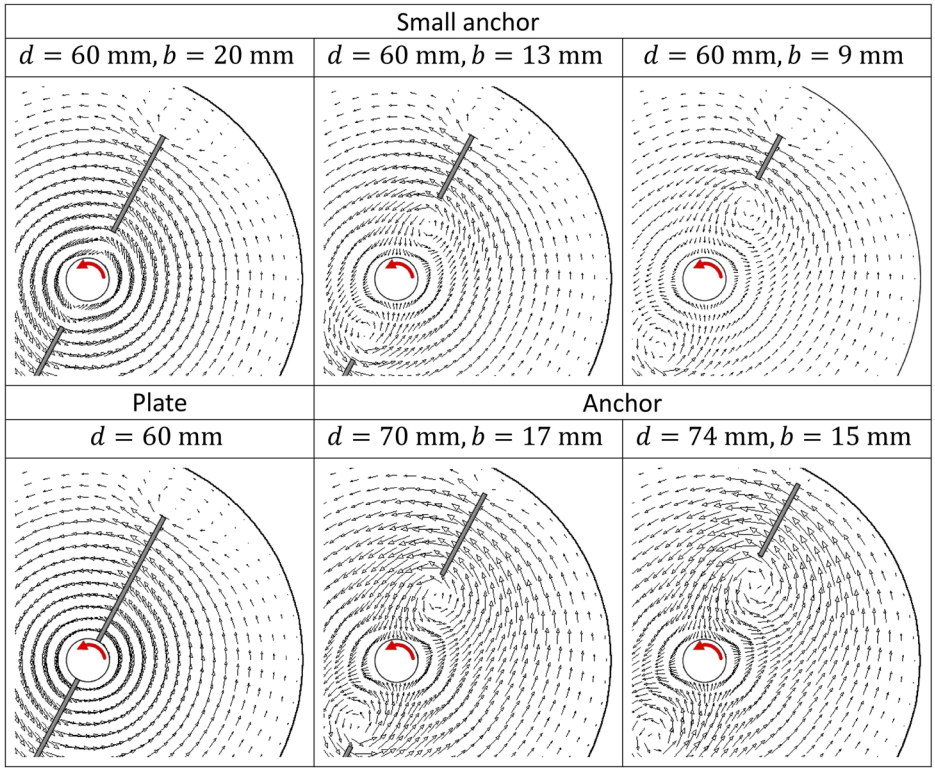

FIG. 13. Two-dimensional velocity fields induced by rotationally reciprocating impellers at the angular orientation $\varphi = \pi/3$.

Furthermore, we care about the flow rate around the impeller plate estimated from the areas unswept by the impeller plate. The inner and outer unswept areas for a $d = 70$ mm anchor impeller are roughly the same, indicating that the flow rate around the blade is balanced. However, the outer area unswept by the $d = 74$ mm anchor impeller was twice that between the inner edge and mixing shaft. As a result, fluid mainly flows through the inner gap, and a small amount of fluid flows through the outer one. Additionally, the asymmetry of central vortex flow for a wider anchor impeller is helpful to avoid the isolated mixing region.

E. Experimental observation of streaklines induced by anchor impellers

To confirm the improvement of fluid mixing by introducing a central clearance, we observed the behavior of the fluid element experimentally as a streakline by injecting tracer fluid continuously from a fixed point. The impeller used in the observation was a plate, a small anchor ($b = 20$ mm), and larger anchor impellers. Figure 14 shows the time series of streaklines for 40 cycles. The last streakline images were superposed with the 180° rotated Poincaré section after 200 cycles to compare with the numerical results. We decided the initial positions of tracer particles for the numerical calculation so that the boundary of the active mixing region and poor mixing zone is distinguishable if it exists. For the plate impeller, a tracer fluid was stretched and folded many times along the vessel wall and finally confined along the wall to form a crescent-shaped colored region. At the same time, the central zone remained uncolored. Additionally, a crescent-shaped region partially gets over the impeller tip, eventually forming the crescent-shaped region. The shape of the colored region agreed well with that of the Poincaré section.

The small anchor impeller also stretches and folds a fluid element, which is not affected by the central clearance. Although the crescent-shaped area has a wavy boundary, the colored region finally gets over the impeller tip, producing a crescent-shaped mixing region as well. After that, the colored fluid reaches the central clearance and then enters the opposite crescent-shaped mixing region [Fig. 14(b) (Multimedia view)-SmallAnchor_Re9.mp4]. The Poincaré section reasonably describes this spreading behavior of a colored fluid; the circular area consists of two crescent-shaped regions without any central poor mixing zone; the density of the tracer particles in one of the crescent-shaped regions is higher than that in the other.

Due to the tracer injection position difference, the tracer fluid is not stretched along the wall when using anchor impellers. Instead, a tracer fluid quickly passes through the central clearance and enters the region on the opposite side where there is no injection point. This behavior is not expectable in the small anchor and plate impellers. In the case of the width of 70 mm, two mixing regions symmetrical about the mixing shaft emerge in the coloring pattern after five cycles. As time goes by, the colored fluid spreads to fill each region, and finally, almost the entire area is colored. Strictly speaking, the shapes of these two patterns are not the same, and the patterns change each other every half cycle of reciprocation. The

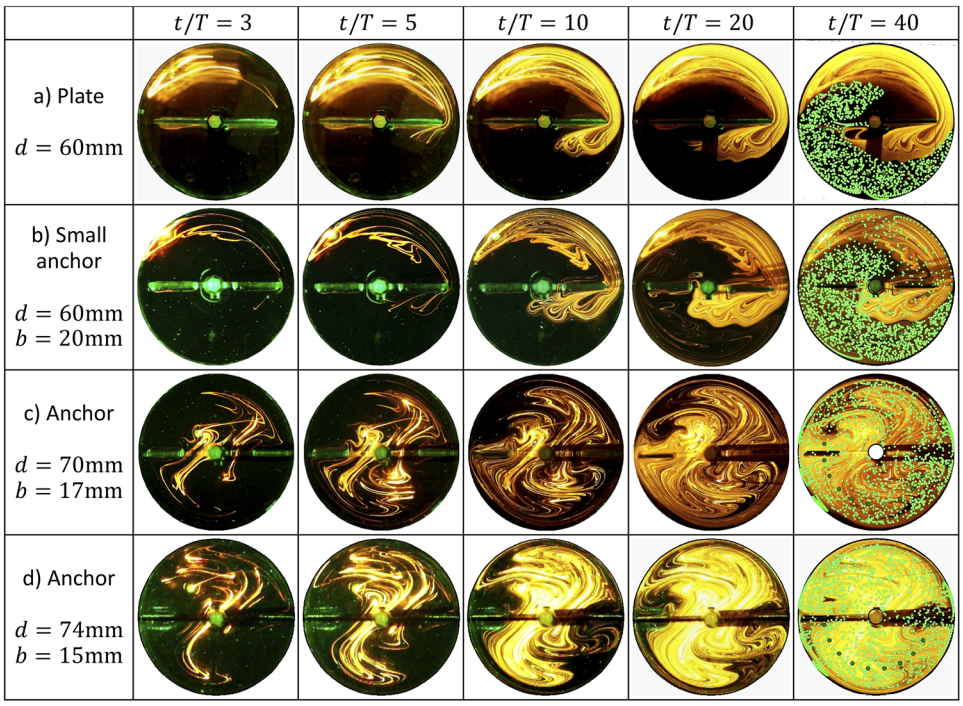

FIG. 14. Development of streaklines induced by plate, small anchor, and anchor impellers. Movies of small anchor and anchor ($d = 74$ mm) are available. (b) and (d) Multimedia views: https://doi.org/10.1063/5.0075750.1 and https://doi.org/10.1063/5.0075750.2

anchor impeller having a width of 74 mm also shows a similar coloring process [Fig. 14(d) (Multimedia view)-Anchor(d74)_Re9.mp4]. The Poincaré cross section and the velocity field predicted that the local mixing ability decreased at the periphery when using the larger anchor impeller. In the visualization experiment for anchor impellers, a tracer fluid injected from the center did not reach the vicinity of the tank wall, making it difficult to emerge poorly mixed regions. To show the difference, we should inject a tracer fluid from the vicinity of the wall, but we did not do that because of the significant effect of the injection nozzle in a narrow wall clearance on the flow. In the larger anchor impeller, a tracer fluid does not reach near the impeller tip due to the weak flow in the gap between the impeller tip and the vessel wall. The result agrees well that green tracer particles are stagnant around the impeller tip, as shown in Fig. 12. The mixing performance of a large plate impeller was best when the volume swept by the impeller plate is equal to the volume flowing in the opposite direction, and we revealed that a geometry that could equally distribute the opposite flow to the inner and outer of the impeller blade is desirable as a rotationally reciprocating anchor impeller.

V. CONCLUSIONS

A rotationally reciprocating plate impeller exhibits excellent mixing performance when the impeller motion generates a well-developed vortex flow. However, under laminar flow conditions with weak vortices, fluid spreads only in the horizontal plane inhomogeneously with producing poor mixing zones in the center of the cylindrical vessel. In this study, we investigated the effect of the center clearance of the plate impeller on the mixing characteristics using anchor impellers. First, the effect of the impeller shape on fluid mixing was investigated based on the velocity field obtained numerically and the Poincaré section constructed using virtual tracer particles. Even when the central clearance was only 10% of the impeller width, the poorly mixed zones disappeared, while isolated mixing regions appeared additionally for sufficiently large central clearances. Although the circular cross section separated into two mixing regions, most tracer particles uniformly spread at the optimum central clearance. We proposed the optimum shape of the anchor impeller by considering the ratio of the area swept and unswept by the impeller. As a result, the optimized anchor impeller showed uniform particle distribution and tiny poorly mixing zones. A comparison of the velocity fields showed that a larger central clearance generates significant flows in the center. However, equalizing the volume flow rate was necessary through the central and wall clearances to create an overall flow. The effectiveness of the optimized anchor impeller was experimentally investigated using a streakline and compared with other impellers. The tracer fluid did not spread evenly in the plate and small anchor impellers. However, the stretching and folding of the fluid element proceeded in the entire region of the vessel when using the optimized anchor impeller. A fluid exchange occurred effectively through the central clearance, resulting in excellent fluid mixing even in laminar flow conditions. The dynamics of the isolated mixing region observed in a small-diameter, narrow-bladed anchor impeller are scientifically intriguing and warrant further study.

The vertical flow disappears in a rotationally reciprocating mixing as the Reynolds number decreases, and fluid mixing occurs only in the horizontal plane. Therefore, it is necessary to create a three-dimensional flow field to improve the mixing performance. Furthermore, at a much smaller Reynolds number, it is necessary to clarify the mechanisms of the segmentation of mixing regions and the formation of poor mixing zones. In the present study, we studied the mixing performance in terms of the spreading behavior of tracer particles and showed that the appropriate combination of central and wall clearances improves the uniformity of mixing performance even at the Reynolds numbers of less than 10. Therefore, we need to confirm the improvement of fluid mixing three-dimensionally at the Reynolds number of 10 or less by introducing axial asymmetry to the anchor impellers and generating vertical fluid flow.

AUTHOR DECLARATIONS

Conflict of Interest

We have no conflicts of interest to declare.

DATA AVAILABILITY

The data that support the findings of this study are available from the corresponding author upon reasonable request.

REFERENCES

[1] J. F. Maingonnat, J. L. Doublier, J. Lefebvre, and G. Delaplace, J. Food Eng. **87**(1), 82 (2008).
[2] L. Bouvier, A. Moreau, A. Line, N. Fatah, and G. Delaplace, J. Food Sci. **76**(5), E384 (2011).
[3] J. Dusting, J. Sheridan, and K. Hourigan, Biotechnol. Bioeng. **94**(6), 1196 (2006).
[4] Y. Lin and J. Thibault, Bioprocess Biosyst. Eng. **36**(5), 603 (2013).
[5] S. Hashimoto, H. Ito, and Y. Inoue, Chem. Eng. Sci. **64**(24), 5173 (2009).
[6] W. M. Yek, M. N. Noui-Mehidi, and R. Parthasarathy, J. Chem. Eng. Jpn. **43**(1), 13 (2010).
[7] S. Wang, J. Wu, and E. Y. Bong, Chem. Eng. Res. Des. **91**(6), 1009 (2013).
[8] M. Farhat, L. Fradette, H. Horiguchi, R. Yatomi, and P. Tanguy, J. Chem. Eng. Jpn. **42**(11), 797 (2009).
[9] K. Nishi, N. Enya, R. Misumi, and M. Kaminoyama, J. Chem. Eng. Jpn. **47**(2), 146 (2014).
[10] S. Wang, J. Wu, and N. Ohmura, Ind. Eng. Chem. Res. **52**(33), 11741 (2013).
[11] M. M. Alvarez, P. E. Arratia, and F. J. Muzzio, Can. J. Chem. Eng. **80**, 546 (2002).
[12] S. Woziwodzki and Ł. Jędrzejczak, Chem. Eng. Res. Des. **89**(11), 2268 (2011).
[13] D. Bulnes-Abundis and M. M. Alvarez, AIChE J. **59**(8), 3092 (2013).
[14] W. M. Yek, M. N. Noui-Mehidi, R. Parthasarathy, S. N. Bhattacharya, J. Wu, N. Ohmura, and N. Nishioka, Can. J. Chem. Eng. **87**(6), 839 (2009).
[15] S. Woziwodzki, Chem. Eng. Technol. **34**(5), 767 (2011).
[16] M. Yoshida, Y. Nagai, K. Yamagiwa, A. Ohkawa, and S. Tezura, Ind. Eng. Chem. Res. **48**, 1665 (2009).
[17] W.-L. Chien, H. Rising, and J. M. Ottino, J. Fluid Mech. **170**, 355 (1986).
[18] P. D. Anderson, O. S. Galaktionov, G. W. M. Peters, F. N. van de Vosse, and H. E. H. Meijer, Int. J. Heat Fluid Flow **21**, 176 (2000).
[19] R. Camassa and S. Wiggins, Phys. Rev. A **43**(2), 774 (1991).
[20] H. Aref, J. Fluid Mech. **143**, 1 (1986).

[21] E. Gouillart, J.-L. Thiffeault, and O. Dauchot, Phys. Rev. Lett. **104**, 204502 (2020).
[22] J. Arrieta, J. H. Cartwright, E. Gouillart, N. Piro, O. Piro, and I. Tuval, PLoS One **10**(7), e0130735 (2015).
[23] S. Senda, Y. Komoda, Y. Hirata, H. Takeda, H. Suzuki, and R. Hidema, J. Chem. Eng. Jpn. **47**(2), 151 (2014).
[24] S. Senda, N. Yamagami, Y. Komoda, Y. Hirata, H. Suzuki, and R. Hidema, J. Chem. Eng. Jpn. **48**(11), 885 (2015).
[25] S. Senda, Y. Komoda, Y. Hirata, H. Takeda, H. Suzuki, and R. Hidema, J. Chem. Eng. Jpn. **49**(4), 341 (2016).
[26] T. Date, Y. Komoda, H. Suzuki, R. Hidema, and K. Suzuki, J. Chem. Eng. Jpn. **51**(2), 159 (2018).
[27] P. A. Tanguy, F. Thibault, and E. B. De La Fuente, Can. J. Chem. Eng. **74**(2), 222 (1996).
[28] M. K. Singh, T. G. Kang, H. E. H. Meijer, and P. D. Anderson, Microfluid. Nanofluid. **5**, 313 (2008).